

1 *Conference Proceedings Paper*

2 **Estimation of surface soil moisture at the intra-plot** 3 **spatial scale by using low and high incidence angles** 4 **TerraSAR-X images**

5 **Rémy Fieuzal** ^{1,*} and **Frédéric Baup** ²

6 Published: date

7 Academic Editor: name

8 ¹ Centre d'Études de la Biosphère (CESBIO), Université de Toulouse, CNES/CNRS/INRAe/IRD/UPS,
9 Toulouse, France; frederic.baup@cesbio.cnes.fr

10 * Correspondence: remy.fieuzal@cesbio.cnes.fr; Tel.: +xx-xxx-xxx-xxxx

11 **Abstract:** The objective of this study is to analyze the capabilities of multi-temporal TerraSAR-X
12 images to estimate the fine-scale SSM variability over bare agricultural plots (at a spatial scale
13 ranging from 80 to 2800 m²). Time series of X-band satellite images were collected over a study site
14 located in southwestern France, together with intra-field measurements of key soil descriptors (i.e.,
15 SSM, surface roughness, soil texture). The large dataset allows independent training and validating
16 steps of a statistical algorithm (random forest), SSM being estimated using images acquired at low
17 at high incidence angles. The level of performances obtained at the plot spatial scale, with R²
18 ranging from 0.64 to 0.67 (depending on the considered incidence angle) and a RMSE close to 5.0
19 m⁻³.m⁻³, are exceeded by those obtained at a finer scale (700 m², corresponding to buffers with a 15
20 m radius). At this intra-plot spatial scale, the estimates based on the low incidence angles images
21 are associated to a R² of 0.69 and a RMSE of 4.89 m⁻³.m⁻³, results slightly lower than performance
22 obtained using high incidence angles images, R² of 0.72 and a RMSE of 4.55 m⁻³.m⁻³. Such
23 magnitude of performance slightly increases over larger intra-plot spatial scales, the values of R²
24 being superior to 0.75 with RMSE lower than 4.20 m⁻³.m⁻³ over areas of 2800 m² (corresponding to
25 buffers with a 30 m radius).

26 **Keywords:** Surface soil moisture; bare soils; TerraSAR-X; random forest; plot spatial scale;
27 intra-plot spatial scale.
28

29 **1. Introduction**

30 Numerous studies have demonstrated the usefulness of SAR satellite images for monitoring
31 subsurface parameters, particularly in an agricultural context during periods without vegetation,
32 where these signals offer the possibility of estimating variables related to the soil (e.g., surface soil
33 moisture, surface roughness, soil texture) [1-3]. The sensitivity of microwave signals to variations in
34 surface soil moisture (SSM) has thus been demonstrated in various studies, and often quantified
35 through empirical relationships [1,4-5]. In these studies, the dynamics of the signals are
36 characterized, but the relationships remain nevertheless limited because they are established under
37 specific conditions (on a limited number of plots or even on a single plot, for specific surface
38 roughness levels, and/or on the basis of images acquired in specific configurations) limiting the
39 possibilities of extrapolation over large areas.

40 To overcome these limitations of application in various contexts, other approaches have been
41 proposed. For example, they are based on the following combination: electromagnetic signal
42 modeling, in order to simulate the diversity of possible cases that can be observed in agricultural
43 conditions, and a statistical inversion method, which is trained on the basis of synthetic data from

44 the modeling [6-7]. The target variable is finally estimated by applying the statistical algorithm to the
45 satellite images. In this approach, the signal modeling step is a central and critical element that will
46 determine the final accuracy of the surface moisture estimates. Different backscattering models can
47 then be used to reproduce SAR signals in bare soil period ([8-10]), while the vegetation component is
48 estimated through the Water Cloud Model [11]. However the soil model's performance are limited,
49 even after modifications by calibration or taking into account the observed biases [12]. An alternative
50 relies on the use of a statistical approach, offering higher performance regarding the estimation
51 backscatter coefficients [13], provided that there are sufficient ground measurements during satellite
52 acquisitions (so that calibration and validation steps can be carried out independently).

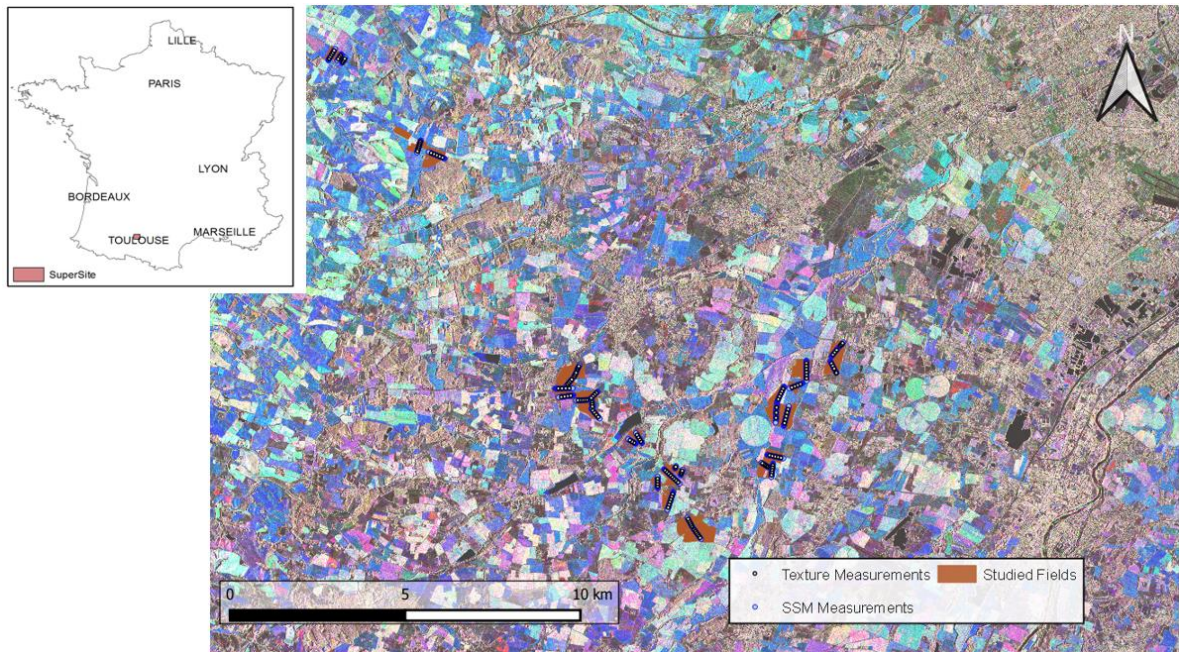
53 Whatever the considered approach, the estimates are derived at spatial scales ranging from the
54 regional (i.e., pixel of several km²) to the plot scale (i.e., area of interest of several hectares), while the
55 possibilities of mapping at intra-plot spatial scale are rarely addressed [1,4-7]. However, this spatial
56 scale is a determining factor in the modulation of agricultural practices, particularly in a context of
57 precision farming. It is therefore necessary to estimate the potential of SAR data for monitoring
58 sub-surface parameters, at spatial scales close to the pixel. Especially in a context where access to
59 SAR images at metric or decametric spatial resolutions is made possible by several satellite missions
60 (e.g., Sentinel-1, Radarsat constellation, Terrasar-X, Tandem-X).

61 The objective of this study is to address the potential of TerraSAR-X data to estimate the surface
62 soil moisture at the intra-plot spatial scale. The mean features of the quasi-synchronously collected
63 ground data and SAR satellite images are described in section 2. The proposed approach is based on
64 a statistical algorithm (i.e., random forest), trained and validated by considering variable areas of
65 interest (i.e., plot and intra-plot spatial scales). The results are analyzed and discussed (section 3),
66 focusing on the overall statistical performances obtained for images acquired at low and high
67 incidence angles.

68 2. Experiments

69 2.1. Study site

70 The network of plots where was conducted the experiment was located in southwestern France
71 (Figure 1). From February to November 2010, in situ measurements of key sub-surface descriptors
72 were regularly collected, synchronously to satellite images (MCM'10 campaign, see [14] for more
73 details). The main characteristics of the study area were: (i) a temperate climate, with an amplitude
74 of mean months temperature near 20°C (observed between winter and summer), and annual
75 cumulative rainfall exceeding 600 mm; (ii) a highly anthropized area, surfaces being mainly
76 allocated to seasonal crops cultivated on more than half of the landscape, (iii) a very fragmented
77 landscape, with plots showing different shapes and sizes (with areas comprised between 1 and 95
78 hectares). In the present study, the focus is on bare soil conditions which were observed after the
79 harvest and before the sowing of the next crop (i.e., in spring and autumn).



80

81 **Figure 1.** Location of the study site (super site) in southwestern France. The network of the surveyed
 82 fields (brown polygons) superimposed on a color-composed TerraSAR-X image acquired in
 83 StripMap mode at HH polarization (Red: 2010/05/20, Green: 2010/08/16, Blue: 2010/11/23). Soil
 84 moisture and texture measurements are represented by blue and black circles respectively.

85 *2.2. Materials*

86 *2.2.1. In situ data*

87 The three key variables having a marked influence on the dynamics of the SAR signals in bare
 88 soil periods, and allowing to characterize the surface horizon were collected on each monitored plot.
 89 The surface roughness was measured after each tillage event, using a 2 meters-long needle
 90 profilometer (composed of 201 needles spaced one centimeter). Two quantitative variables were
 91 derived from the couples of profiles recorded parallel and perpendicular to the direction of the
 92 tillage of the plot. The values of root mean square height (hrms) and the correlation length (l_c)
 93 showed large variation intervals (varying from 0.5 to 6.9 cm, and 1.1 to 16.5 cm, respectively),
 94 consistent with the observed surface conditions (with smooth to very rough surfaces). Surface soil
 95 moisture (i.e., top soil layer of 0-5 cm) and texture geo-located measurements were performed along
 96 the same transects for each field. The fractions of clay, silt, and sand were derived from 2 to 8 points
 97 performed on each plot, consisting in 16 core samples within a circle of 15 m of diameter and a depth
 98 of 25 cm. A total of 146 points were collected, showing the dominance of the silt fraction within the
 99 study area (52% of silt and 24% of clay and sand, for average values) and an important variation of
 100 texture conditions with fractions between 22 and 77% for the silt, between 9 and 58% for the clay,
 101 and between 4 and 53% for the sand. The monitoring of SSM was performed using portable probes
 102 (ML2x from ThetaProbe), delivering a signal in mV which was converted in volumetric moisture
 103 (using the calibration relationship established by [14]). The regular measurements of SSM were
 104 collected quasi-synchronously with satellite acquisitions (time lag between in situ measurements
 105 and satellite acquisitions of less than one day for the majority of cases), allowing to characterize soil
 106 in a wide range of moisture conditions (from dry to saturated), characterized by values of SSM
 107 ranging from 3.2 to 34.9%.

108 *2.2.2. TerraSAR-X satellite data*

109 The German satellite TerraSAR-X operating in the X-band ($f = 9.65$ GHz, $\lambda = 3.1$ cm) provided
 110 the 21 microwave images (Table 1). They were acquired at low (27.3°) or high (53.3°) incidence
 111 angles (11 and 10 images respectively) in HH polarization. Two beam modes (SpotLight and
 112 StripMap) characterized by a pixel spacing ranging from 1.5 to 2.75 m [15] were used. All images
 113 were calibrated, the backscattering coefficients were finally average at the plot scale and considering
 114 six buffers with a radius ranging from 5 to 30 m (corresponding to areas from ~ 80 to ~ 2800 m²).

115 **Table 1.** Mean features of the TerraSAR-X images acquired with SpotLight (SL) and StripMap (SM)
 116 modes.

Mode	Acquisition Date	Orbit Pass	Incidence	Pixel
			Angle ($^\circ$)	size (m)
Spotlight	03/05/10 ; 05/21/10 ; 07/15/10 ; 08/17/10 ; 09/30/10	D	53.3	1.5
	10/11/10 ; 10/22/10 ; 11/02/10 ; 11/13/10 ; 11/24/10			
StripMap	02/21/10 ; 03/26/10 ; 05/09/10 ; 05/20/10 ; 07/14/10	D	27.3	2.75
	08/16/10 ; 09/29/10 ; 10/10/10 ; 10/21/10 ; 11/12/10 ; 11/23/10			

117 2.3. Method

118 The statistical algorithm proposed by [16] was used to estimate SSM, by considering the
 119 following inputs as explanatory variables: the backscattering coefficients and the incidence angles of
 120 the SAR images, the fractions of clay and sand, and the soil root mean square height (hrms) and
 121 correlation length (lc) collected in the parallel and perpendicular directions. Random forest has been
 122 widely used in different fields, being particularly appropriate in multi-factorial context to model
 123 non-linear relationships. The targeted variable is derived from a weighted mean of an ensemble of
 124 estimations, obtained from independent decision trees trained on different set of samples. Such a
 125 procedure limits the problems of over-adjustment or the noise influence on data, and provides a
 126 high stability of results.

127 In the present study, independent cases were considered accordingly to the considered spatial
 128 scale, that was plot or intra-plot. Six buffer area were taken into account by considering the
 129 geo-location of texture measurements as reference and radius ranging from 5 to 30 m (corresponding
 130 to areas from ~ 80 to ~ 2800 m²). These areas of interest were used to extract the SAR satellite signals
 131 and to select the corresponding SSM measurements.

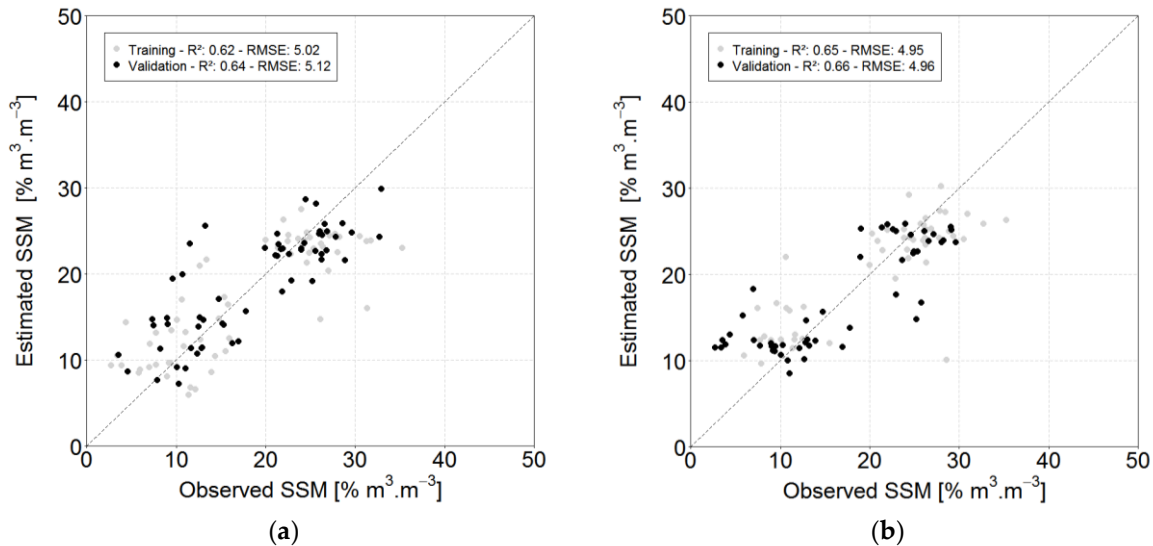
132 Whatever the considered spatial scale, the dataset was randomly partitioned into two subsets.
 133 The statistical algorithm was calibrated on the training set and validated on the independent test set.
 134 This procedure was repeated ten times. Finally, the average values of the coefficient of
 135 determination (R^2) and the root mean square error (RMSE) were derived from the comparison
 136 between the observed and estimated values of the SSM.

137 3. Results and discussions

138 3.1. Overall performances obtained at the plot spatial scale

139 The estimated values of SSM are compared to in situ measurements showing the independent
 140 subsets of samples used during the training and validation steps (in grey and black, respectively)
 141 (Figure 2). The levels of performances are close regardless the considered incidence angle, with
 142 RMSE of 5.12 and 4.96 % m³.m⁻³, and R^2 of 0.64 and 0.66 (values obtained for the validation subset of
 143 samples). A quasi-similar magnitude of values is observed during the training step, pointing out the
 144 high stability of results when using RF algorithm. The level of accuracy and in particular the
 145 correlation values may appear to be limited, however these results are consistent with a number of
 146 past studies performed over bare soils, using X-band SAR signal and empirical or semi-empirical

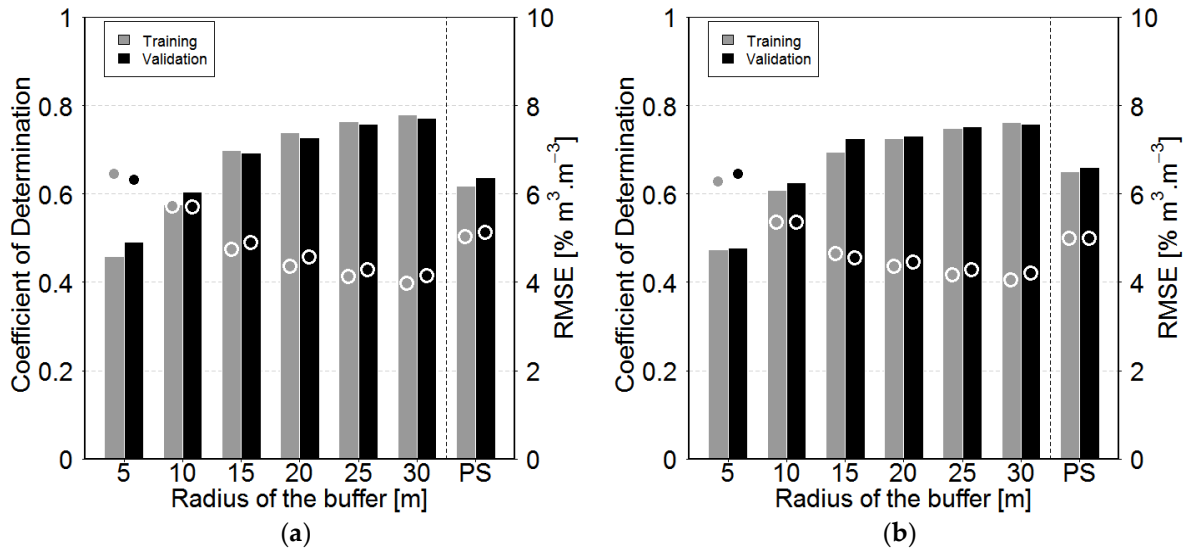
147 models [1,4-5,7]. Although these approaches are different from the one implemented here, the
 148 performance levels are equivalent to those obtained with the statistical approach, the best results
 149 showing SSM estimates with an R^2 ranging from 0.64 to 0.79 and an RMSE when presented varying
 150 between 2.81 and 4.09 $\text{m}^3\cdot\text{m}^{-3}$. Moreover, in our case the approach is applied over a wider soil
 151 roughness domain (hrms of 3.9 cm in the previous case compared to 6.9 cm in the present case), and
 152 independently to images acquired at two contrasting incidence angles (i.e., at 27.3 and 53.3°),
 153 without observing any noticeable difference on the level of performance. The absence of angular
 154 effect constitutes an advantage of the proposed method, offering interesting prospects for estimating
 155 SSM using satellite images with various configurations.



156 **Figure 2.** Comparison between in situ measurements of surface soil moisture and estimates derived
 157 from TerraSAR-X images acquired at 27.3° (a) or 53.3° (b). The grey and black dots represent the
 158 estimations performed considering the training or validation subsets of samples, respectively.

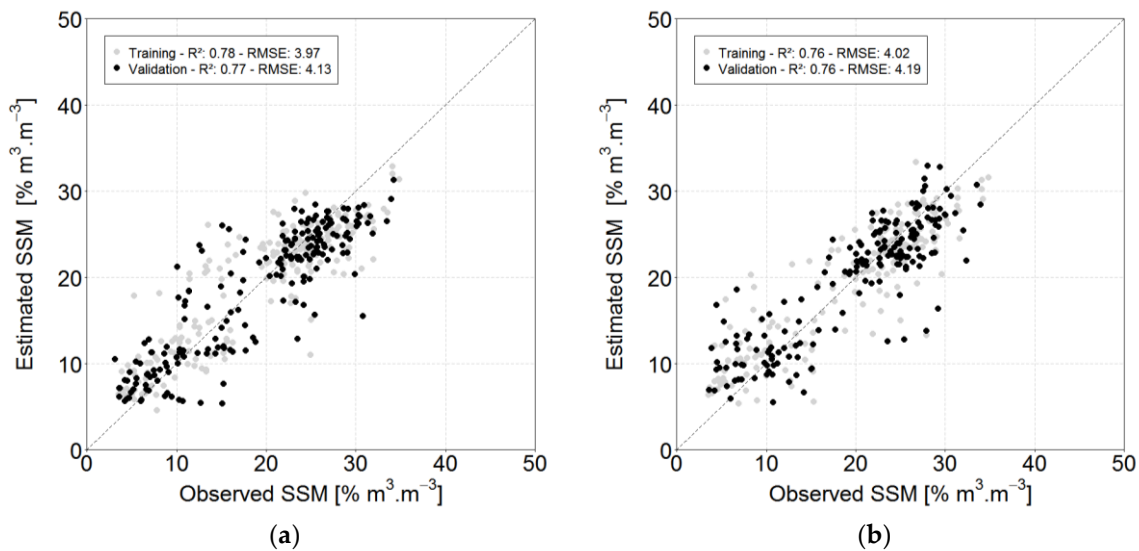
159 *3.2. Evolution of the statistical performance at the intra-plot spatial scale*

160 The Figure 3 presents the statistical performances (R^2 and RMSE) obtained by comparing the
 161 values of SSM estimated using the statistical approach to ground measurements for circular buffers
 162 ranging from 5 to 30 m, together with results obtained at the plot scale. The performance increase in
 163 correlation from 0.46 to 0.78, while the error decreases from 6.45 to 3.97% $\text{m}^3\cdot\text{m}^{-3}$, when considering
 164 the 5 and 30m buffers. This gain in performance has a non linear behavior and becomes weak when
 165 the radius of the buffer reaches 20m. This phenomenon is mainly explained by the specificities of the
 166 SAR signal, and in particular by the radiometric resolution. In a previous study, [17] characterize the
 167 radiometric resolution for the two TerraSAR-X beam modes used in the present study. For the
 168 considered intra-plot spatial scales, the values of radiometric resolution shift from 0.71 to 0.13 dB
 169 and from 1.14 to 0.21 dB, for the SL and SM beam modes respectively. The non-linear performance
 170 gain observed with the increase in buffer size appears to be consistent with the exponential decrease
 171 in radiometric resolution values. Statistical performance is thus very close for buffers greater than
 172 20m radius (radiometric resolution values being almost similar). Moreover, weaker performances
 173 obtained at plot scale highlight the fact that SSM measurements performed ponctually do not
 174 represent significantly the surface state at the plot scale.



175 **Figure 3.** Evolution of the statistical performances (coefficients of determination and root mean
 176 square errors, bars and dots respectively) with the buffer's size and at the plot spatial scale (PS), for
 177 the training (grey) or validation (black) subsets of samples, for SSM estimates derived from TS-X
 178 images acquired at low (27.3°) and high (53.3°) incidence angles (a and b, respectively).

179 Figure 4 presents a comparison between the estimated and in situ measurements of SSM values
 180 for the buffer of 30 m. At this spatial scale, a high level of performance is observed on both training
 181 and validation steps, and whatever the considered incidence angle. The values of R² exceeds 0.75
 182 while the RMSE on SSM estimates is lower than 4.2% m³.m⁻³. SSM estimates, however, are associated
 183 with wide dispersion, although performance levels obtained at this spatial scale exceed previous
 184 results obtained at the spatial scale of the plot [1,4-5,7].



185 **Figure 4.** Comparison between estimated and observed SSM for a buffer with a radius of 30 m, for
 186 TS-X images acquired at low (27.3°) and high (53.3°) incidence angles (a and b, respectively). The
 187 grey or black colors represent the estimations performed considering the training or validation
 188 subsets of samples, respectively.

189 **5. Conclusions**

190 The present study takes advantage of a dense network of georeferenced in situ measurements
 191 collected synchronously with the regular acquisition of X-band SAR images, to address the potential

192 of high spatial resolution TerraSAR-X data for surface soil moisture estimation at the intra-plot scale.
193 Results based on a statistical algorithm are obtained from images with low and high incidence
194 angles (i.e., 27.3 and 53.3°), showing performance levels consistent with the literature at plot scale
195 and particularly promising results at the intra-plot scale (R^2 superior to 0.75 and RMSE lower than
196 $4.20 \text{ m}^{-3} \cdot \text{m}^{-3}$ over areas of 2800 m^2 regardless the incidence angle).

197 The actual or planned satellite missions offer a wide range of possibilities that should be tested
198 with the method presented here, by considering images acquired at different frequencies, at
199 contrasting angles of incidence, or with different polarization states. The only constraint lies in the
200 availability of data, especially in situ, in order to be able to implement the statistical approach.
201 Moreover, the characteristics of the satellite sensors, as well as the beam modes of image acquisition,
202 condition the SAR signal that needs to be tested to determine the possibilities for intra-plot scale
203 studies offered by other satellite missions.
204

205 **Acknowledgments:** Authors would like to thank especially Space Agencies for their support and confidence
206 they have in this project (CNES, ESA, and DLR). Many thanks to farmers and people who helped for collecting
207 ground data.

208 **Author Contributions:** The authors contributed equally to the various steps required to complete this study.
209 All authors have read and agreed to the published version of the manuscript.

210 **Conflicts of Interest:** The authors declare no conflict of interest.

211 References

- 212 1. Baghdadi, N.; Aubert, M.; Zribi, M. Use of TerraSAR-X data to retrieve soil moisture over bare soil
213 agricultural fields. *IEEE Trans. Geosci. Remote Sens. Lett.*, **2012**, 9(3), 512-516.
- 214 2. Maleki, M.; Amini, J.; Notarnicola, C. Soil roughness retrieval from TerraSar-X data using neural network
215 and fractal method. *Advances in Space Research*, **2019**, 64(5), 1117-1129.
- 216 3. Zribi, M.; Kotti, F.; Lili-Chabaane, Z.; Baghdadi, N.; Ben Issa, N.; Amri, R.; Amri, B.; Chehbouni, A. Soil
217 texture estimation over a semiarid area using TerraSAR-X radar data. *IEEE Trans. Geosci. Remote Sens. Lett.*
218 **2012**, 9, 353-357.
- 219 4. Aubert, M.; Baghdadi, N.; Zribi, M.; Douaoui, A.; Loumagne, C.; Baup, F.; El Hajj, M.; Garrigues, S.
220 Analysis of TerraSAR-X data sensitivity to bare soil moisture, roughness, composition and soil crust.
221 *Remote Sens. Environ.* **2011**, 115, 1801-1810.
- 222 5. Gorrab, A.; Zribi, M.; Baghdadi, N.; Mougenot, B.; Chabaane, Z.L. Potential of X-Band TerraSAR-X and
223 COSMO-SkyMed SAR data for the assessment of physical soil parameters. *Remote Sens.* **2015**, 7, 747-766.
- 224 6. Mirsoleimani, H.R.; Sahebi, M.R.; Baghdadi, N.; El Hajj, M. Bare soil surface moisture retrieval from
225 Sentinel-1 SAR data based on the calibrated IEM and Dubois models using neural networks. *Sensors* **2019**,
226 19, 3209.
- 227 7. El Hajj, M.; Baghdadi, N.; Zribi, M.; Belaud, G.; Cheviron, B.; Courault, D.; Charron, F. Soil moisture
228 retrieval over irrigated grassland using X-band SAR data. *Remote Sens. Environ.* **2016**, 176, 202-218.
- 229 8. Oh, Y.; Sarabandi, K.; Ulaby, F.T. An empirical model and an inversion technique for radar scattering from
230 bare soil surfaces. *IEEE Trans. Geosci. Remote Sens.* **1992**, 30, 370-381.
- 231 9. Dubois, P.C.; van Zyl, J.; Engman, T. Measuring soil moisture with imaging radars. *IEEE Trans. Geosci.*
232 *Remote Sens.* **1995**, 33, 915-926.
- 233 10. Fung, A.K.; Li, Z.; Chen, K.-S. , Backscattering from a randomly rough dielectric surface. *IEEE Trans.*
234 *Geosci. Remote Sens.* **1992**, 30, 356-369.
- 235 11. Attema, E. P. W.; Ulaby, F. T. Vegetation modeled as a water cloud. *Radio Science*, **1978**, 13, 357-364.
- 236 12. Fieuzal, R.; Baup, F. Improvement of bare soil semiempirical radar backscattering models (Oh and Dubois)
237 with SAR multi-spectral satellite data (at X, C and L bands). *Advances in Remote Sens.*, **2016**, 5(4), 296-314,
238 2016.
- 239 13. Fieuzal, R.; Baup, F. Statistical estimation of backscattering coefficients in X-band over bare agricultural
240 soils," *2020 Mediterranean and Middle-East Geoscience and Remote Sensing Symposium (M2GARSS)*, Tunis,
241 Tunisia, **2020**, 302-305.

- 242 14. Baup, F.; Fieuzal, R.; Marais-Sicre, C.; Dejoux, J.-F.; le Dantec, V.; Mordelet, P.; Claverie, M.; Hagolle, O.;
243 Lopes, A.; Keravec, P.; Ceschia, E.; Mialon, A.; Kidd, R. MCM'10: An experiment for satellite multi-sensors
244 crop monitoring from high to low resolution observations. *2012 IEEE International Geoscience and Remote*
245 *Sensing Symposium*, Munich, **2012**, 4849-4852.
- 246 15. Breit, H.; Fritz, T.; Balss, U.; Lachaise, M.; Niedermeier, A.; Vonavka, M. TerraSAR-X SAR processing and
247 products. *IEEE Trans. Geosci. Remote Sens.* **2010**, *48*, 27-40.
- 248 16. Breiman, L. Random Forests. *Machine Learning*, **2001**, *45*(1), 5-32.
- 249 17. Fieuzal, R.; Marais, S.C.; Baup, F. Estimation of corn yield using multi-temporal optical and radar satellite
250 data and artificial neural networks. *Int. J. Appl. Earth Obs. Geoinf.* **2017**, *57*, 14–23.



© 2020 by the authors; licensee MDPI, Basel, Switzerland. This article is an open access article distributed under the terms and conditions of the Creative Commons by Attribution (CC-BY) license (<http://creativecommons.org/licenses/by/4.0/>).